Available online at www.sciencedirect.com
SCIENCE DIRECT®
International Journal of Heat and Mass Transfer 48 (2005) 4174–4189
International Journal of HEAT and MASS TRANSFER
www.elsevier.com/locate/ijhmt

On the control of solidification using magnetic fields and magnetic field gradients

Baskar Ganapathysubramanian, Nicholas Zabaras *

Materials Process Design and Control Laboratory, Sibley School of Mechanical and Aerospace Engineering, 188 Frank H.T. Rhodes Hall, Cornell University, Ithaca, NY 14853-3801, USA

Received 27 May 2004; received in revised form 21 January 2005

Abstract

Solidification from the melt to near net shape is a commonly used manufacturing technique. The fluid flow patterns in the melt affect the quality of the final product. By controlling the flow behavior, the final solidified material can be suitably affected. Most of the magnetic field approaches to melt flow control rely on the application of a constant magnetic field. A constant magnetic field results in the Lorentz force which is used to damp and control the flow. However, simultaneous application of a magnetic gradient results in the Kelvin force along with the Lorentz force. This can be used for better control of the melt flow resulting in higher crystal quality. In the present work, a computational method for the design of solidification of a conducting material is addressed. The control parameter in the design problem is the time history of the imposed magnetic field. A steady, constant magnetic gradient is also maintained during the process. The design problem is posed as an unconstrained optimization problem. The adjoint method for the inverse design of continuum processes is adopted. Examples of designing the time history of the imposed magnetic field for the directional growth of various materials are presented to demonstrate the developed formulation.

Keywords: Magnetic gradients; Kelvin force; Magneto-hydrodynamics; Solidification; Crystal growth

1. Introduction

Solidification from the melt is the most commonly used means of manufacturing to near net shape for most materials, especially metals and semi-conductors. The quality of the final product implicitly depends on the process of solidification. For example, during crystal growth, heat flux fluctuations from the melt to the crystal produce a cycle of crystallization and remelting at the interface. This cycle produces dislocations and other microscopic defects in the crystal. Convective flow in the melt leads to fluctuations in the solute concentration in the crystal which results in the formation of residual stresses in the cooled crystal [1, Chapter 14]. Controlling the solidification process is therefore a means of controlling the quality/properties of the final product.

All metals and most semi-conductor melts have a relatively high electrical conductivity and are subject to electromagnetic forces when moving in a magnetic field. This concept has been used to damp natural convection in the melt through the application of constant magnetic

* Corresponding author. Tel.: +1 607 255 9104; fax: +1 607 255 1222.
E-mail address: zabaras@cornell.edu (N. Zabaras).
URL: http://mpdc.mae.cornell.edu/ (N. Zabaras).

0017-9310/$ - see front matter © 2005 Elsevier Ltd. All rights reserved.
doi:10.1016/j.ijheatmasstransfer.2005.04.027

Nomenclature

B_0	initial magnetic field
$\mathbf{b}_f$	body force
$b(t)$	non-dimensional magnetic field
$\mathbf{B}$	magnetic field
c	solute concentration in the fluid
c_0	reference concentration
C_p	specific heat of the fluid
$\mathbf{C}$	sensitivity solute concentration
c_i	initial concentration in the melt
D	solute diffusivity
$\mathbf{e}_i$	unit vector in the ith direction
$\mathbf{E}$	induced electric field
F	sensitivity temperature operator
F^*	adjoint temperature operator
g	gravity constant
G	sensitivity velocity operator
G^*	adjoint velocity operator
H	sensitivity concentration operator
H^*	adjoint concentration operator
Ha	Hartmann number
J	sensitivity potential operator
J^*	adjoint potential operator
$\mathbf{J}$	electric current density
k	thermal conductivity of the melt
L_H	latent heat of fusion
Le	Lewis number
L	characteristic length
$\mathbf{M}$	magnetization
m	slope of the liquidus
$\mathbf{n}$	unit normal to the interface
n_{sd}	number of space dimensions
p	pressure
Pr	Prandtl number
R_k	ratio of thermal conductivities
R_α	ratio of thermal diffusivities
Ra_T	thermal Rayleigh number
Ra_C	solutal Rayleigh number
R^d	Euclidean space of dimension d
$S(b)$	cost functional
Ste	Stefan number
t	non-dimensional time
T_i^*	initial temperature in the solid
T_i	initial temperature in the melt
T_0	reference temperature
T	temperature in the fluid
$\mathbf{v}$	velocity of the fluid
$\mathbf{v}_f$	velocity of the solid–liquid interface
$\mathbf{V}$	sensitivity velocity
$\mathbf{V}_f$	sensitivity interface velocity

Greek symbols

α	thermal diffusivity of the melt, the step length in the optimization algorithm
β_T, β_C	coefficient of expansion, thermal and solutal
γ	non-dimensional Kelvin force, the optimal step size in the CGM
Γ	boundary of the physical domain
γRa_T	magnetic Rayleigh number
ΔT	reference temperature drop
Δb	perturbation to the magnetic field
Δc	reference concentration drop
$D_{\Delta b}$	directional derivative along Δb
δ	$\frac{c_0}{\Delta c}$
η	adjoint potential
θ_i	initial temperature of the melt
θ_i^*	initial temperature of the solid
θ_0	freezing temperature
θ	non-dimensional temperature
Θ	sensitivity temperature
κ	partition coefficient
μ_m	permeability of free space
ν	kinematic viscosity
ξ	adjoint concentration
π	adjoint pressure
Π	sensitivity pressure
ρ_l	density of the melt
ρ_0	reference density
σ, σ_m	stress tensor, electrical conductivity
Σ	sensitivity of the stress tensor
ϕ	electric potential
Φ	sensitivity potential
χ	mass magnetic susceptibility
χ_m	magnetic susceptibility
ψ	adjoint temperature
Ω	physical domain
ω	adjoint velocity

fields. The application of magnetic fields is also known to stabilize both flow and temperature oscillations in the melt and thereby represents a promising opportunity to obtain an improved crystal quality [2,3]. The effects of a constant magnetic field on melt convection have been previously investigated by several authors [4–7]. The effects of a strong vertical magnetic field on convection and segregation in the vertical Bridgeman crystal growth process was considered by Ben Hadid et al. [6,7], while Kim et al. [8] studied the effects of a magnetic field on the horizontal Bridgeman growth. Recently, Gunzberger et al. [9] estimated the optimal magnitude of the constant magnetic field necessary for the suppression of turbulent flow in the melt. Even though there is a

therapeutic effect of the application of a constant magnetic field there are some disadvantages to its use during solidification:

- A constant magnetic field suppresses thermo-solutal flow, but the inter-dendritic flows and macro-segregation patterns are not significantly affected by the magnetic field [10].
- Any significant convection damping requires prohibitively large magnetic fields.
- The magnetic field must be oriented in a specific direction relative to the bulk flow for the Lorentz force to take effect.

To circumvent these problems, the use of different types of magnetic fields on solidification were investigated. The effect of a Rotating Magnetic Field (RMF) on crystal growth and solidification was investigated by Patzold et al. [11] and Roplekar and Dantzig [12]. Galindo et al. [13] studied the effects of a rotating as well as a travelling magnetic field on crystal growth processes. The use of a RMF results in suppression of convection but fluctuations in temperature and concentration leading to striation patterns in the crystal still persist. Recently, Evans et al. [14] demonstrated that a magnetic gradient could be used to damp convection in any material, conducting or non-conducting. A magnetic gradient subjects the fluid to the Lorentz and Kelvin forces [15]. A suitable combination of these forces can result in suppression of fluctuations along with convection damping. In an earlier work [16], the authors investigated the effect of magnetic gradients on the quality of the crystal (pure material/dilute mixture). A constant magnetic gradient superimposed on a uniform magnetic field caused substantial reduction in convection and resulted in a much better crystal. In [17], the authors investigate the design of non-homogeneous magnetic fields to control the solidification and crystal growth of non-conducting (e.g. biological) materials. In the present work, the effect of the variation in the magnetic field superimposed on a constant gradient on growth of a conducting material is investigated. The time history of the magnetic field that needs to be applied during growth to obtain a convectionless (microgravity-like) environment in the melt is estimated.

To the best of our knowledge, this is the first time that (mathematical) control of solidification is affected through the variation in magnetic fields. As stated earlier, the time history of the magnetic field is the design parameter that has to be estimated. Various solution methods based on finite or infinite dimensional optimization techniques can be developed to calculate the unknown design parameters. A particularly effective method is the infinite-dimensional regularization scheme. This method, which involves the formulation of an appropriate continuum adjoint problem that allows the analytical calculation of the exact gradient of the objective function, is extensively used in the present work. The sequencing of the various sections in this paper is as follows. The equations governing the underlying physics of the problem of interest are presented in Section 2. The inverse solidification problem is posed as a functional optimization problem and the adjoint system of equations is derived in Section 3. In Section 4, the developed formulation is applied to various examples. Finally, in Section 5, a summary of the work and some conclusions are provided.

2. The direct solidification problem

Let Ω be a closed bounded region in $R^{n_{sd}}$, where n_{sd} is the number of spatial dimensions, with a piece-wise smooth boundary Γ. The region is filled with an incompressible, conducting fluid. At time $t = 0$, a part of the boundary is cooled below the freezing temperature of the fluid and solidification begins along that boundary. Two-dimensional applications are considered in this paper but the formulation presented is dimension-independent. Let us denote the solid region by Ω_s and the liquid region by Ω_l. These regions share a common solid–liquid interface boundary Γ_I. As seen in Fig. 1, the region Ω_l has a boundary Γ_l which consists of Γ_I (the solid–liquid interface), Γ_{ol} (the mold wall on the liquid side), Γ_{bl} (the bottom boundary of the liquid domain) and Γ_{tl} (the top boundary of the liquid domain). Similarly Ω_s has boundary Γ_s, which consists of Γ_I, Γ_{os}, Γ_{bs} and Γ_{ts}.

An externally applied (spatially varying) magnetic field acts on the whole domain Ω. An assumption that the induced magnetic field is very small compared to the external magnetic field is made (the ratio of the induced to the external field, the magnetic Prandtl number, is extremely small for semi-conductors and metals

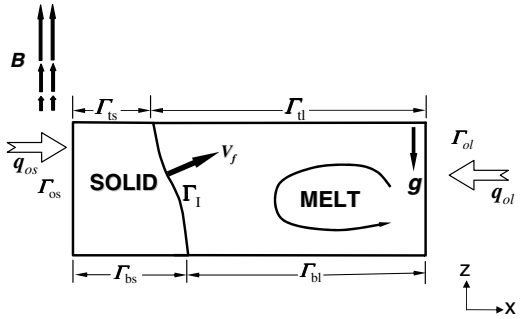

Fig. 1. Schematic of the directional solidification system. A time-varying magnetic field **B** and a constant magnetic field gradient $\frac{\partial B}{\partial z}$ are applied in the z direction.

[1]). The action of the magnetic field on the moving fluid results in the generation of induced currents in the fluid [18]. The electrical resistance of the material causes heating of the fluid element. This heating, called the Joule heating is neglected after an order of magnitude analysis reveals that this term is small compared to the other terms in the energy equation. With the classical MHD assumptions of non-relativistic flow and quasi-magneto-statics, the electro-magnetic force on the system is written as follows [19]:

$$\mathbf{f}_{\mathrm{em}} = \mathbf{J} \times \mathbf{B} + (\nabla \mathbf{B})\mathbf{M} \tag{1}$$

where $\mathbf{J}$ is the current density and $\mathbf{M}$ is the magnetization given as

$$\mathbf{M} = \frac{\chi_{\mathrm{m}}}{\mu_{\mathrm{m}}(1+\chi_{\mathrm{m}})}\mathbf{B} \approx \frac{\chi_{\mathrm{m}}}{\mu_{\mathrm{m}}}\mathbf{B} \tag{2}$$

where χ_{m} is the magnetic susceptibility of the material and μ_{m} is the permeability of free space.

The time variation of the magnetic field is small enough for the quasi-magneto-static assumption to be valid. The current density $\mathbf{J}$ can be represented through the extended form of Ohm's law [1] as follows:

$$\mathbf{J} = \sigma_e(\mathbf{E} + \mathbf{v} \times \mathbf{B}) \tag{3}$$

where $\mathbf{E}$ is the induced electric field. Under the assumption of small magnetic Prandtl number, $\mathbf{E}$ is restricted to the form $\mathbf{E} = -\nabla\phi$, where ϕ is the electric potential [20]. Following Tagawa et al. [21,22], the Boussinesq approximation applied to the Kelvin term results in Eq. (1) becoming

$$\mathbf{f}_{\mathrm{em}} = \sigma_{\mathrm{e}}(-\nabla\phi + \mathbf{v} \times \mathbf{B}) \times \mathbf{B} + \gamma\rho_0 g\beta(T - T_0) \tag{4}$$

where $\gamma = \gamma_i \mathbf{e}_i$ with

$$\gamma_i \equiv \frac{\chi \sum_{j=1}^{3} \frac{\partial B_i}{\partial x_j} B_j}{\mu_{\mathrm{m}} g} \tag{5}$$

and χ is the mass magnetic susceptibility of the material. For diamagnetic fluids, the mass susceptibility is independent of temperature but the form of the Kelvin force in Eq. (4) arises from the density changes with temperature. As can be seen from Eq. (4), uniform magnetic field damping depends on the action of the Lorentz force which is proportional to the vector product of the flow velocity and the field strength. It therefore has a decreasing influence with decreasing flow velocity and so is ill-fitted to the further damping of very weak flows. In comparison to the Lorentz force, the Kelvin force is independent of the fluid velocity and it can lead to substantial suppression of velocity with moderate magnetic fields.

Remark 1. The Kelvin force can be controlled independently in different ways. For example, by varying the direction and/or magnitude of the magnetic field or, by varying the magnitude of each of the components of the gradient tensor. The independent control of the external magnetic field and its gradient can be achieved in Magnetic Resonance Imaging (MRI) machines that require independently controllable magnetic fields and magnetic gradients [23] for reliable imaging of human tissue. Rapid progress in MRI imaging has resulted in the commercial production of linear magnetic fields producing gradient coils [24].

Based on Remark 1, in the context of solidification and crystal growth control using magnetic fields, it is possible to control the Kelvin force term in twelve independent ways. But in the present work, the variation in the Kelvin force is assumed to be only due to changes in the magnetic field. That is, the magnetic gradients are kept fixed and any variation in the Kelvin force is due to corresponding changes to the magnetic field $\mathbf{B}(t)$. Further, since the aim of using a magnetic field is to control the convection causing forces, the magnetic field from now on is considered to be in the direction of buoyancy i.e. $\mathbf{B} = B\mathbf{e}_z$ and $\nabla\mathbf{B} = \frac{\partial B}{\partial z}\mathbf{e}_z$. For this case, we simply denote γ_z as γ. Extension to different orientations of the magnetic field and magnetic gradients is very straightforward. The applied field $B(t)$ is non-dimensionalized with the initial field of magnitude B_0 (unless is otherwise stated), and the non-dimensionalized field is referred to as $b(t) = \frac{B(t)}{B_0}$. The Kelvin force is therefore given as $\gamma_0 b\rho_0\beta(T - T_0)g\mathbf{e}_g$, where γ_0 is $\frac{\chi B_0 \frac{\partial B}{\partial z}}{\mu g}$ and the applied magnetic field gradient $\frac{\partial B}{\partial z}$ is here taken as constant. In the notation above, $\mathbf{e}_{\mathrm{g}}$ is the unit vector in the direction of gravity, i.e. $\mathbf{e}_g = -\mathbf{e}_z$.

For clarity of analysis and to understand the effect of competing complex processes, the system is analyzed in a non-dimensional form. The characteristic scales are taken as L^2/α for time and α/L for velocity. The dimensionless temperature is defined as $\theta \equiv (T - T_0)/\Delta T$, Similarly, the dimensionless concentration is taken as $c \equiv (c - c_0)/\Delta c$. The electric potential ϕ is non-dimensionalized with αB_0. Henceforth, ϕ refers to the non-dimensionalized electric potential unless otherwise stated.

The basic equations that govern the evolution of the directionally solidifying system are given in Box I. In the equations, R_k and R_α are the ratios of the thermal conductivity and thermal diffusivity, respectively, of the solid to the melt. The governing equations are given in terms of the following dimensionless groups: Prandtl number, ($Pr \equiv \nu/\alpha$), Lewis number ($Le \equiv \alpha/D$), Stefan number ($Ste \equiv (C_{\mathrm{p}}\Delta T)/L_H$), thermal Rayleigh number ($Ra_{\mathrm{T}} \equiv g\beta_{\mathrm{T}}\Delta T L^3/\nu\alpha$), solutal Rayleigh number ($Ra_{\mathrm{C}} \equiv g\beta_{\mathrm{C}}\Delta c L^3/\nu\alpha$), magnetic Rayleigh number ($\gamma Ra_{\mathrm{T}}, \gamma \equiv \frac{\gamma B^2 \frac{\partial B}{\partial z}}{\mu g}$) and Hartmann number ($Ha \equiv (\frac{\sigma_e}{\rho_1 \nu})^{1/2} B_0 L$).

Box I. Direct problem to define $\mathbf{v}(\mathbf{x}, t; b)$, $\theta(\mathbf{x}, t; b)$, $c(\mathbf{x}, t; b)$ and $\phi(\mathbf{x}, t; b)$

- Melt region

$$\nabla \cdot \mathbf{v} = 0, \quad (\mathbf{x}, t) \in \Omega_l(t) \times [0, t_{\max}]$$

$$\frac{\partial \mathbf{v}}{\partial t} + \mathbf{v} \cdot \nabla \mathbf{v} = -\nabla p + Pr \nabla^2 \mathbf{v} - Ra_T Pr \theta_l \mathbf{e}_g + Ra_T Pr \gamma_0 b \theta_l \mathbf{e}_g + Ra_C Prc \mathbf{e}_g + Ha^2 Prb^2 [-\nabla \phi + \mathbf{v} \times \mathbf{e}_B] \times \mathbf{e}_B, \quad (\mathbf{x}, t) \in \Omega_l(t) \times [0, t_{\max}]$$

$$\frac{\partial c}{\partial t} + \mathbf{v} \cdot \nabla c = Le^{-1} \nabla^2 c, \quad (\mathbf{x}, t) \in \Omega_l(t) \times [0, t_{\max}]$$

$$\nabla^2 \phi = \nabla \cdot (\mathbf{v} \times \mathbf{e}_B), \quad (\mathbf{x}, t) \in \Omega_l(t) \times [0, t_{\max}]$$

$$\frac{\partial \theta_l}{\partial t} + \mathbf{v} \cdot \nabla \theta_l = \nabla^2 \theta_l, \quad (\mathbf{x}, t) \in \Omega_l(t) \times [0, t_{\max}]$$

$$\frac{\partial \theta_l}{\partial n} = 0, \ \frac{\partial c}{\partial n} = 0, \quad (\mathbf{x}, t) \in (\Gamma_l(t) - \Gamma_I(t)) \times [0, t_{\max}]$$

$$\mathbf{v} = \mathbf{0}, \ \frac{\partial \phi}{\partial n} = 0, \quad (\mathbf{x}, t) \in \Gamma_l(t) \times [0, t_{\max}]$$

$$\mathbf{v} = \mathbf{0}, \ c = c_i, \ \theta = \theta_i, \quad \mathbf{x} \in \Omega_l(t = 0)$$

- Solid zone

$$\frac{\partial \theta_s}{\partial t} = R_\alpha \nabla^2 \theta_s, \quad (\mathbf{x}, t) \in \Omega_s(t) \times [0, t_{\max}]$$

$$\theta_s = \theta_i^*, \quad \mathbf{x} \in \Omega_s(t = 0)$$

$$\frac{\partial \theta_s}{\partial n} = 0, \quad (\mathbf{x}, t) \in (\Gamma_s - \Gamma_{os}) \times [0, t_{\max}]$$

$$\theta_s = \theta_{s2}, \quad (\mathbf{x}, t) \in \Gamma_{os} \times [0, t_{\max}]$$

- Interface

$$R_k \frac{\partial \theta_s}{\partial t} - \frac{\partial \theta_l}{\partial t} = Ste^{-1} \mathbf{v}_\Gamma \cdot \mathbf{n}, \quad (\mathbf{x}, t) \in \Gamma_I(t) \times [0, t_{\max}]$$

$$\theta = \theta_0 + mc, \quad (\mathbf{x}, t) \in \Gamma_I(t) \times [0, t_{\max}]$$

$$\frac{\partial c}{\partial n} = Le(k - 1)(c + \delta) \mathbf{v}_\Gamma \cdot \mathbf{n}, \quad (\mathbf{x}, t) \in \Gamma_I(t) \times [0, t_{\max}]$$

3. Definition of the inverse design solidification problem

3.1. Design objectives

In the conclusions in Chapter 5 in [1], Hurle et al. comment on the ideal conditions for crystal growth. They state the best results can be anticipated to come from the combined use of microgravity and a magnetic field, wherein the microgravity would reduce the steady convective flows to a minimum with the magnetic field damping any small fluctuations. The effect of the spatially varying magnetic field is similar to this situation. The Kelvin force causes a state of reduced gravity while the Lorentz damps out small fluctuations. Keeping this in view, the objective of the design procedure is to produce a growth that is purely diffusion-dominated. The reduction of convection in the melt can be achieved by applying the magnetic field in such a way so as to reduce the convection causing buoyant forces. The definition of the design solidification problem can now be stated as follows:

With given magnetic field gradient $\frac{\partial B}{\partial z}$, find the time history of the superimposed magnetic field $b(t)$, such that the directional solidification defined by the initial boundary value problem (IBVP) in Box I proceeds with negligible convection over the entire time domain.

3.2. Controlled solidification of pure materials and dilute alloys: analytical design solution

In this subsection, an analytical expression for the time history of the imposed magnetic field is determined. Convection, in the case of a pure material or a dilute alloy, is due to the thermal gradients that occur during the solidification. At any time instant, the net body force acting on a fluid volume in the melt region is the sum of the thermal buoyant force, the Kelvin force and the Lorentz force. But the Lorentz force implicitly depends on the velocity of the fluid volume. At the beginning of the growth, when the whole melt is in a quiescent state, only the first two of the afore mentioned three body forces act on the fluid volume.

$$\mathbf{b}_\Gamma = -Ra_T Pr \theta_l(\mathbf{x}, t) \mathbf{e}_g + Ra_T Pr \gamma_0 b \theta_l(\mathbf{x}, t) \mathbf{e}_g \tag{6}$$

If $\gamma_0 b$ is chosen to be equal to 1, then both the terms on the right-hand side of the above equation become equal and cancel to zero. In other words, if the field is chosen such that

$$\gamma_0 = \frac{\chi B_0 \frac{\partial B}{\partial z}}{\mu g} = 1.0, \quad b(t) = 1.0 \tag{7}$$

then because of the absence of any convection causing forces, the growth at early times would be diffusion-dominated. This would ensure that there is no (significant) Lorentz force acting on the fluid volume. In other words, initially the effect of Lorentz force is negligible because of the stagnant fluid, but at later times the proper choice of γ_0 enforces negligible convection, and hence zero Lorentz force. Therefore, given the magnitude of the applied magnetic gradient $\frac{\partial B}{\partial z}$, the optimal value of the imposed magnetic field is $B_0 = \frac{\mu g}{\chi \frac{\partial B}{\partial z}}$. In this case, $b(t)$ remains constant through out the growth. In general, time varying $b(t)$ can be achieved by varying the power (current) input to the magnetic coils [1,23].

3.3. Controlled solidification of binary alloys: a functional optimization framework

In this subsection, the solidification of a conducting mixture in the general case is considered. Electromagnetic as well as solutal and thermal induced convection is dominant during the solidification process. The non-dimensional governing equations are given in Box I. To achieve a diffusion-based growth, the combined magnetic field and magnetic field gradient must be chosen in such a way so as to negate the effects of the thermal and convective buoyancy. With the particular assumptions of constant magnetic gradient introduced earlier, the objective is restated in terms of $b(t) \in L_2[0, t_{\max}]$. In particular, we are looking for an optimal solution $\bar{b}(t) \in L_2[0, t_{\max}]$ such that

$$S(\bar{b}) \leqslant S(b) \quad \forall b(t) \in L_2[0, t_{\max}] \tag{8}$$

where

$$\begin{aligned} S(b) &= \frac{1}{2}\|\mathbf{v}(\mathbf{x}, t; b)\|^2_{L_2(\Omega_l \times [0, t_{\max}])} \\ &= \frac{1}{2}\int_0^{t_{\max}} \int_{\Omega_l(t)} \mathbf{v}(\mathbf{x}, t; b) \cdot \mathbf{v}(\mathbf{x}, t; b)\, \mathrm{d}\Omega\, \mathrm{d}t \end{aligned} \tag{9}$$

with the melt velocity $\mathbf{v}(x, t; b)$ defined from the solution of the problem in Box I with the magnetic field $b(t)$ as a function parameter and with a given superimposed magnetic gradient, $\frac{\partial B}{\partial z}$. In the following discussion, we will use $(f, g)_{L_2(\Omega_l \times [0, t_{\max}])}$ or simply (f, g) to denote the dot product of any (scalar or vector) functions f and g in $L_2(\Omega_l \times [0, t_{\max}])$.

The main difficulty with the above optimization problem is the calculation of the gradient $S'(b(t))$ of the cost functional in $L_2[0, t_{\max}]$. Introducing the directional derivative $D_{\Delta b}S(b) \equiv (S'(b), \Delta b)_{L_{2[0,t_{\max}]}}$ of $S(b)$, and using the definition of the cost functional, we can write the following:

$$\begin{aligned} D_{\Delta b}S(b) &\equiv (S'(b), \Delta b)_{L_2[0, t_{\max}]} \\ &= (\mathbf{v}(\mathbf{x}, t; b), \mathbf{V}(\mathbf{x}, t; b, \Delta b))_{L_2(\Omega_l \times [0, t_{\max}])} \end{aligned} \tag{10}$$

where the sensitivity velocity field $\mathbf{V}(\mathbf{x}, t; b, \Delta b) \equiv D_{\Delta b}\mathbf{v}(\mathbf{x}, t; b)$, the sensitivity temperature field $\Theta(\mathbf{x}, t; b, \Delta b) \equiv D_{\Delta b}\theta(\mathbf{x}, t; b)$, sensitivity concentration field $C(\mathbf{x}, t; b, \Delta b) \equiv D_{\Delta b}c(\mathbf{x}, t; b)$ and sensitivity potential field $\Phi(\mathbf{x}, t; b, \Delta b) \equiv D_{\Delta b}\phi(\mathbf{x}, t; b)$ are defined as the linear Δb parts of $\theta(\mathbf{x}, t; b)$, $\mathbf{v}(x, t; b)$, $c(\mathbf{x}, t; b)$ and $\phi(x, t; b)$, respectively, calculated at b:

$$\begin{aligned} \theta(\mathbf{x}, t; b + \delta b) &= \theta(\mathbf{x}, t; b) + \Theta(\mathbf{x}, t; b, \Delta b) + \mathrm{O}(\|\Delta b\|^2_{L_2}) \\ \mathbf{v}(\mathbf{x}, t; b + \Delta b) &= \mathbf{v}(\mathbf{x}, t; b) + \mathbf{V}(\mathbf{x}, t; b, \Delta b) + \mathrm{O}(\|\Delta b\|^2_{L_2}) \\ c(\mathbf{x}, t; b + \Delta b) &= c(\mathbf{x}, t; b) + C(\mathbf{x}, t; b, \Delta b) + \mathrm{O}(\|\Delta b\|^2_{L_2}) \\ \phi(\mathbf{x}, t; b + \Delta b) &= \phi(\mathbf{x}, t; b) + \Phi(\mathbf{x}, t; b, \Delta b) + \mathrm{O}(\|\Delta b\|^2_{L_2}) \end{aligned}$$

As is clear from Eq. (10), the calculation of the gradient $S'(b)$ requires the evaluation of the adjoint to the sensitivity of the velocity operator. The definition of the sensitivity problem is addressed next followed by the derivation of the corresponding adjoint operators.

3.3.1. Governing equations for the sensitivity problem

Taking the directional derivatives of the governing equations of Box I in the direction of Δb and calculated at the direct fields $\theta(\mathbf{x}, t; b)$, $c(\mathbf{x}, t; b)$, $\phi(\mathbf{x}, t; b)$ and $\mathbf{v}(\mathbf{x}, t; b)$ corresponding to the imposed field $b(t)$ results in a linear sensitivity solidification problem that can be used to evaluate the fields $\Theta(\mathbf{x}, t; b, \Delta b)$, $C(\mathbf{x}, t; b, \Delta b)$, $\Phi(\mathbf{x}, t; b, \Delta b)$ and $\mathbf{V}(\mathbf{x}, t; b, \Delta b)$. This sensitivity problem is summarized in Box II, where $\Sigma(\mathbf{x}, t; b, \Delta b)$ and $\Pi(\mathbf{x}, t; b, \Delta b)$ are used to denote the directional derivatives (sensitivities) of stress $\sigma(\mathbf{x}, t; b)$ and pressure $p(\mathbf{x}, t; b)$, respectively.

Remark 2. It is important to notice that the domain of definition $\Omega_l(t)$ of the governing equations in the melt as given in Box I is itself time varying, and also depends on the control parameter $b(t)$. In deriving the sensitivity equations of Box II, the governing equations of Box I are linearized (with respect to $b(t)$) by considering the contribution of the sensitivity with respect to $b(t)$ of the front velocity (and thus of the domain) only in the Stefan temperature condition and the concentration condition at the interface. It has been verified with extensive numerical testing [17], that the system of equations in Box II indeed represents the evolution of the sensitivity fields governing the solidification process. Sensitivity calculations based on the direct analysis for two nearby magnetic fields ($b(t)$ and $b(t) + \Delta b(t)$) also revealed that the sensitivity $\mathbf{V}_f$ of the front velocity $\mathbf{v}_f$ was negligible compared to other sensitivity variables.

3.3.2. Adjoint equations

The derivation of the adjoint operators is given in this subsection. The calculation of the gradient of the objective function requires the appropriate evaluation of the adjoint operators to the sensitivity operators. The adjoint temperature is represented as ψ while ω, ξ and η represent the adjoint velocity, adjoint concentration and adjoint electric potential, respectively. The sensitivity operators for the thermal, fluid flow, concentration and electric potential problems are denoted by F, G, H and J. The adjoint operators F^*, G^*, H^*, J^* are defined from the following Lagrange identities:

$$\begin{aligned} (\mathsf{F}^*\psi, \Theta)_{L_2(\Omega_l \times [0, t_{\max}])} &= (\psi, \mathsf{F}\Theta)_{L_2(\Omega_l \times [0, t_{\max}])} \equiv 0 \\ (\mathsf{G}^*\omega, \mathbf{V})_{L_2(\Omega_l \times [0, t_{\max}])} &= (\omega, \mathsf{G}\mathbf{V})_{L_2(\Omega_l \times [0, t_{\max}])} \equiv 0 \\ (\mathsf{H}^*\xi, C)_{L_2(\Omega_l \times [0, t_{\max}])} &= (\xi, \mathsf{H}C)_{L_2(\Omega_l \times [0, t_{\max}])} \equiv 0 \\ (\mathsf{J}^*\eta, \Phi)_{L_2(\Omega_l \times [0, t_{\max}])} &= (\eta, \mathsf{J}\Phi)_{L_2(\Omega_l \times [0, t_{\max}])} \equiv 0 \end{aligned}$$

Consider first the concentration operator H^*. We start with

$$(\xi, \mathsf{H}C) = \left(\xi, \frac{\partial C}{\partial t} + \mathbf{v}\cdot\nabla C + \mathbf{V}\cdot\nabla c - Le^{-1}\nabla^2 C\right) = 0 \tag{11}$$

Following the derivations given in [17], the above equation can be written as

$$\begin{aligned}&\left(\xi, \frac{\partial C}{\partial t} + \mathbf{v}\cdot\nabla C + \mathbf{V}\cdot\nabla c - Le^{-1}\nabla^2 C\right)\\ &= \left(C, -\frac{\partial \xi}{\partial t} - \mathbf{v}\cdot\nabla\xi - Le^{-1}\nabla^2\xi\right) + (\xi, \mathbf{V}\cdot\nabla c)\\ &\quad - Le^{-1}(\xi\nabla C - C\nabla\xi, \mathbf{n})_{\Gamma_1}\\ &= 0\end{aligned} \tag{12}$$

Box II. Sensitivity problem to define $\mathbf{V}(\mathbf{x}, t; b, \Delta b)$, $\Theta(\mathbf{x}, t; b, \Delta b)$, $C(\mathbf{x}, t; b, \Delta b)$ and $\Phi(\mathbf{x}, t; b, \Delta b)$

- Melt region

$$\nabla\cdot\mathbf{V} = 0, \quad (\mathbf{x}, t) \in \Omega_l(t)\times[0, t_{\max}]$$

$$\begin{aligned}&\frac{\partial \mathbf{V}}{\partial t} + \mathbf{V}\cdot\nabla\mathbf{v} + \mathbf{v}\cdot\nabla\mathbf{V}\\ &\quad = -\nabla\cdot\Sigma - Ra_T Pr(1-\gamma_0 b)\Theta\mathbf{e}_g + Ra_c PrC\mathbf{e}_g\\ &\qquad + Ra_T Pr\Delta b\gamma_0\theta\mathbf{e}_g + Ha^2 Prb^2[-\nabla\Phi + \mathbf{V}\times\mathbf{e}_B]\times\mathbf{e}_B\\ &\qquad + 2Ha^2 Prb\Delta b[-\nabla\phi + \mathbf{v}\times\mathbf{e}_B]\times\mathbf{e}_B,\\ &\quad (\mathbf{x}, t) \in \Omega_l(t)\times[0, t_{\max}]\end{aligned}$$

$$\Sigma = -\Pi\mathbf{I} + Pr[\nabla\mathbf{V} + (\nabla\mathbf{V})^T], \ (\mathbf{x}, t) \in \Omega_l(t)\times[0, t_{\max}]$$

$$\begin{aligned}&\frac{\partial C}{\partial t} + \mathbf{v}\cdot\nabla C + \mathbf{V}\cdot\nabla c = Le^{-1}\nabla^2 C,\\ &\quad (\mathbf{x}, t) \in \Omega_l(t)\times[0, t_{\max}]\end{aligned}$$

$$\frac{\partial\Theta}{\partial t} + \mathbf{v}\cdot\nabla\Theta + \mathbf{V}\cdot\nabla\theta = \nabla^2\Theta, \ (\mathbf{x}, t) \in \Omega_l(t)\times[0, t_{\max}]$$

$$\nabla^2\Phi = \nabla\cdot(\mathbf{V}\times\mathbf{e}_B), \quad (\mathbf{x}, t) \in \Omega_l(t)\times[0, t_{\max}]$$

$$\frac{\partial\Theta_l}{\partial n} = 0, \ \frac{\partial C}{\partial n} = 0, \quad (\mathbf{x}, t) \in (\Gamma_l(t) - \Gamma_I(t))\times[0, t_{\max}]$$

$$\mathbf{V} = \mathbf{0}, \ \frac{\partial\Phi}{\partial n} = 0, \quad (\mathbf{x}, t) \in \Gamma_l(t)\times[0, t_{\max}]$$

$$\mathbf{V} = \mathbf{0}, \ C = 0, \ \Theta = 0, \ \Phi = 0 \quad \mathbf{x} \in \Omega_l(t=0)$$

- Interface

$$R_k\frac{\partial\Theta_s}{\partial n} - \frac{\partial\Theta_l}{\partial n} = Ste^{-1}\mathbf{V}_f\cdot\mathbf{n}, \quad (\mathbf{x}, t) \in \Gamma_I(t)\times[0, t_{\max}]$$

$$\Theta = m\mathbf{C}, \quad (\mathbf{x}, t) \in \Gamma_I(t)\times[0, t_{\max}]$$

$$\frac{\partial C}{\partial n} = Le(k-1)(c+\delta)\mathbf{V}_f\cdot\mathbf{n} + Le(k-1)C\mathbf{v}_f\cdot\mathbf{n}$$

where the notation $(\mathbf{f}, \mathbf{n})_{\Gamma_1} = \int_{\Gamma_1}\int_0^{t_{\max}}\mathbf{f}\cdot\mathbf{n}\,\mathrm{d}\Gamma\,\mathrm{d}t$ is introduced for any vector function $\mathbf{f}$. By adding and subtracting $(C, \omega\cdot\mathbf{e}_g)$ from the above equation, the following is derived:

$$\begin{aligned}&\left(C, -\frac{\partial\xi}{\partial t} - \mathbf{v}\cdot\nabla\xi - Le^{-1}\nabla^2\xi + \omega\cdot\mathbf{e}_g\right) + (\xi, \mathbf{V}\cdot\nabla c)\\ &\quad - (C, \omega\cdot\mathbf{e}_g) - Le^{-1}(\xi\nabla C - C\nabla\xi, \mathbf{n})_{\Gamma_I} = 0\end{aligned} \tag{13}$$

The adjoint concentration operator is then defined as follows:

$$\mathsf{H}^*\xi \equiv -\frac{\partial\xi}{\partial t} - \mathbf{v}\cdot\nabla\xi - Le^{-1}\nabla^2\xi + \omega\cdot\mathbf{e}_g = 0 \tag{14}$$

We enforce $\xi(\mathbf{x}, t; b)$ to be the solution of the adjoint equation defined by Eq. (14) with zero flux $\frac{\partial\xi}{\partial n}$ on all boundaries of Γ_1 except the interface Γ_I, where the following equation is applied:

$$\begin{aligned}\frac{\partial\xi}{\partial n} &= \frac{\xi\frac{\partial C}{\partial n}}{C}\\ &= \xi\frac{Le(k-1)(c+\delta)\mathbf{V}_f\cdot\mathbf{n} + Le(k-1)C\mathbf{v}_f\cdot\mathbf{n}}{C}\end{aligned} \tag{15}$$

where $\frac{\partial C}{\partial n}$ on Γ_I was written using the expression given in Box II. Neglecting the sensitivity of the front velocity (see Remark 2) leads to the following boundary condition for the adjoint concentration:

$$\frac{\partial\xi}{\partial n} = \xi Le(k-1)\mathbf{v}_f\cdot\mathbf{n} \tag{16}$$

Using the adjoint concentration operator in Eq. (14) along with Eq. (16), the following coupling criterion for the concentration and velocity fields is obtained from Eq. (13):

$$(\xi, \mathbf{V}\cdot\nabla c) = (C, \omega\cdot\mathbf{e}_g) \tag{17}$$

A similar procedure is followed for the adjoint temperature operator $\mathscr{F}^*$. Beginning with

$$\begin{aligned}(\psi, \mathsf{F}\Theta) &\equiv \left(\psi, \frac{\partial\Theta}{\partial t} + \mathbf{v}\cdot\nabla\Theta + \mathbf{V}\cdot\nabla\theta - \nabla^2\Theta\right)\\ &= 0\end{aligned} \tag{18}$$

and following steps similar to the derivation of the concentration operator (see [17]) gives

$$\begin{aligned}&\left(\psi, \frac{\partial\Theta}{\partial t} + \mathbf{v}\cdot\nabla\Theta + \mathbf{V}\cdot\nabla\theta - \nabla^2\Theta\right)\\ &= \left(\Theta, -\frac{\partial\psi}{\partial t} - \mathbf{v}\cdot\nabla\psi - \nabla^2\psi\right) + (\psi, \mathbf{V}\cdot\nabla\theta)\\ &\quad + (\psi\nabla\Theta - \Theta\nabla\psi, \mathbf{n})_{\Gamma_I}\\ &= 0\end{aligned} \tag{19}$$

where we have used the initial conditions for Θ and the zero flux boundary conditions of Θ on $(\Gamma_1 - \Gamma_I)$. Further, boundary conditions of zero flux for the adjoint temperature in $(\Gamma_1 - \Gamma_I)$ is used in the above derivation.

A final condition on the adjoint temperature field was also introduced in the derivation of Eq. (19) as follows:

$$\psi(\mathbf{x}, t_{\max}; b) = 0, \quad \mathbf{x} \in \Omega_l(t_{\max}) \tag{20}$$

Let us add and subtract $(\Theta, (1-\gamma_0 b)\omega \cdot \mathbf{e}_g)$ from the above equation to derive the following:

$$\begin{aligned}&\left(\Theta, -\frac{\partial \psi}{\partial t} - \mathbf{v}\cdot\nabla\psi - \nabla^2\psi + (1-\gamma_0 b)\omega\cdot\mathbf{e}_g\right)\\ &\quad + (\psi, \mathbf{V}\cdot\nabla\theta) + (\psi\nabla\Theta - \Theta\nabla\psi, \mathbf{n})_{\Gamma_I}\\ &\quad - (\Theta, (1-\gamma_0 b)\omega\cdot\mathbf{e}_g) = 0\end{aligned} \tag{21}$$

The adjoint temperature operator is defined as

$$\mathsf{F}^*\psi \equiv -\frac{\partial\psi}{\partial t} - \mathbf{v}\cdot\nabla\psi - \nabla^2\psi + (1-\gamma_0 b)\omega\cdot\mathbf{e}_g = 0 \tag{22}$$

The boundary conditions are zero flux $\frac{\partial\psi}{\partial n} = 0$, on all parts of Γ_1 except the interface Γ_I where the following equation is satisfied:

$$\Theta\frac{\partial\psi}{\partial n} = \psi\frac{\partial\Theta}{\partial n} = \psi\left(\frac{\partial\Theta_s}{\partial n} - Ste^{-1}\mathbf{V}_f\cdot\mathbf{n}\right) \tag{23}$$

where $\frac{\partial\Theta}{\partial n}$ at the left side of the freezing front was expressed above using the sensitivity of the Stefan condition given in Box II. The temperature boundary conditions in the solid region for the direct problem are independent of the control parameter. That is, the thermal boundary conditions remain the same for growth under $b(t)$ as well as $b(t)+\Delta b(t)$. This results in homogeneous boundary conditions for the sensitivity solid temperature, leading to a trivial solution for the solid sensitivity temperature evolution. This together with neglecting $\mathbf{V}_f$ (Remark 2) gives us a condition of zero flux for the adjoint temperature on the interface boundary. Using Eqs. (21)–(23) leads to the following coupling criterion for the temperature and velocity fields:

$$(\psi, \mathbf{V}\cdot\nabla\theta) = (\Theta, (1-\gamma_0 b)\omega\cdot\mathbf{e}_g) \tag{24}$$

The electric potential operator J^* is derived as follows:

$$(\eta, \mathsf{J}\Phi) = (\eta, \nabla^2\Phi - \nabla\cdot(\mathbf{V}\times\mathbf{e}_B)) = 0 \tag{25}$$

Applying Green's theorem to Eq. (25) and applying the zero flux boundary conditions for the sensitivity potential and forcing a zero flux condition on the boundary for the adjoint potential gives

$$(\Phi, \nabla^2\eta) - (\mathbf{V}, \nabla\cdot(\eta\times\mathbf{e}_B)) = 0 \tag{26}$$

We now add and subtract $(\Phi, b^2\nabla\cdot(\omega\times\mathbf{e}_B))$ to Eq. (26)

$$\begin{aligned}&(\Phi, \nabla^2\eta - b^2\nabla\cdot(\omega\times\mathbf{e}_B)) + (\Phi, b^2\nabla\cdot(\omega\times\mathbf{e}_B))\\ &\quad - (\mathbf{V}, \nabla\cdot(\eta\times\mathbf{e}_B)) = 0\end{aligned} \tag{27}$$

The adjoint electric potential is defined as

$$\mathsf{J}^*\eta \equiv \nabla^2\eta - b^2\nabla\cdot(\omega\times\mathbf{e}_B) = 0 \tag{28}$$

The derivation results in the following coupling criterion for the electric potential and velocity fields:

$$(\Phi, b^2\nabla\cdot(\omega\times\mathbf{e}_B)) = (\mathbf{V}, \nabla\cdot(\eta\times\mathbf{e}_B)) \tag{29}$$

The velocity operator G^* is derived below:

$$\begin{aligned}(\omega, \mathsf{G}\mathbf{V}) \equiv &\left(\omega, \frac{\partial\mathbf{V}}{\partial t} + \mathbf{V}\cdot\nabla\mathbf{v} + \mathbf{v}\cdot\nabla\mathbf{V} - \nabla\cdot\Sigma\right.\\ &+ Ra_T Pr(1-\gamma_0 b)\Theta\mathbf{e}_g - Ra_c PrC\mathbf{e}_g\\ &- Ra_T Pr\gamma_0\Delta b\theta\mathbf{e}_g - Ha^2 Prb^2[-\nabla\Phi + \mathbf{V}\times\mathbf{e}_B]\times\mathbf{e}_B\\ &\left.-2Ha^2 Prb\Delta b[-\nabla\phi + \mathbf{v}\times\mathbf{e}_B]\times\mathbf{e}_B\right)\\ &= 0\end{aligned} \tag{30}$$

Sampath and Zabaras [20] have derived a similar equation related to magneto-convection. After some simple but tedious algebra Eq. (30) becomes

$$\begin{aligned}&\left(\mathbf{V}, -\frac{\partial\omega}{\partial t} - \mathbf{v}\cdot\nabla\omega + \omega\cdot\nabla\mathbf{v}^T - \nabla\pi - Pr\nabla^2\omega\right.\\ &\quad \left. - Ha^2 Prb^2[\mathbf{e}_B(\omega\cdot\mathbf{e}_B) - \omega]\right) + (\omega, (1-\gamma_0 b)Ra_T Pr\Theta\mathbf{e}_g)\\ &\quad - (\omega, Ra_c PrC\mathbf{e}_g + Ha^2 Prb^2[-\nabla\Phi + \mathbf{V}\times\mathbf{e}_B]\times\mathbf{e}_B)\\ &\quad - (\Phi, Ha^2 Prb^2\nabla\cdot(\omega\times\mathbf{e}_B)) - (\omega, Ra_T Pr\gamma_0\Delta b\theta\mathbf{e}_g)\\ &\quad - (\omega, 2Ha^2 Prb\Delta b[-\nabla\phi + \mathbf{v}\times\mathbf{e}_B]\times\mathbf{e}_B) = 0\end{aligned} \tag{31}$$

where π is the adjoint pressure. The adjoint velocity is constrained such that $\nabla\cdot\omega = 0$ in $\Omega_l(t)\times[0, t_{\max}]$ and $\omega(\mathbf{x}, t_{\max}) = 0$ in $\Omega_l(t_{\max})$. Using the coupling equations derived for the concentration, temperature and electric potential operators (Eqs. (17), (24), (29)), Eq. (31) can be simplified into the following form:

$$\begin{aligned}&\left(\mathbf{V}, -\frac{\partial\omega}{\partial t} - \mathbf{v}\cdot\nabla\omega + \omega\cdot\nabla\mathbf{v}^T - \nabla\pi - Pr\nabla^2\omega\right.\\ &\quad + Ra_T Pr\psi\nabla\theta - Ra_c Pr\xi\nabla c - Ha^2 Pr\nabla\cdot(\eta\times\mathbf{e}_B)\\ &\quad \left. - Ha^2 Prb^2[\mathbf{e}_B(\omega\cdot\mathbf{e}_B) - \omega]\right) - (\omega, Ra_T Pr\gamma_0\Delta b\theta\mathbf{e}_g)\\ &\quad - (\omega, 2Ha^2 Prb\Delta b[-\nabla\phi + \mathbf{v}\times\mathbf{e}_B]\times\mathbf{e}_B) = 0\end{aligned} \tag{32}$$

Adding and subtracting $(\mathbf{V}, Ra_T Pr\mathbf{v})$ to Eq. (32) gives

$$\begin{aligned}&\left[\mathbf{V}, -\frac{\partial\omega}{\partial t} - \mathbf{v}\cdot\nabla\omega + \omega\cdot\nabla\mathbf{v}^T - \nabla\pi - Pr\nabla^2\omega\right.\\ &\quad + Ra_T Pr\psi\nabla\theta - Ra_T Pr\mathbf{v} - Ra_c Pr\xi\nabla c\\ &\quad \left. - Ha^2 Prb^2[\mathbf{e}_B(\omega\cdot\mathbf{e}_B) - \omega] - Ha^2 Pr\nabla\cdot(\eta\times\mathbf{e}_B)\right]\\ &\quad + (\mathbf{V}, Ra_T Pr\mathbf{v}) - (\omega, Ra_T Pr\gamma_0\Delta b\theta\mathbf{e}_g)\\ &\quad - (\omega, 2Ha^2 Prb\Delta b[-\nabla\phi + \mathbf{v}\times\mathbf{e}_B]\times\mathbf{e}_B) = 0\end{aligned} \tag{33}$$

The adjoint velocity operator is defined as

$$\begin{aligned}\mathsf{G}^*\omega \equiv &-\frac{\partial\omega}{\partial t} - \mathbf{v}\cdot\nabla\omega + \omega\cdot\nabla\mathbf{v}^T - \nabla\pi - Pr\nabla^2\omega\\ &+ Ra_T Pr\psi\nabla\theta - Ra_T Pr\mathbf{v} - Ra_c Pr\xi\nabla c\\ &- Ha^2 Prb^2[\mathbf{e}_B(\omega\cdot\mathbf{e}_B) - \omega] - Ha^2 Pr\nabla\cdot(\eta\times\mathbf{e}_B)\\ &= 0\end{aligned} \tag{34}$$

By forcing $\omega(\mathbf{x}, t; b)$ to satisfy Eq. (34) along with no-slip boundary conditions at the boundaries, Eq. (30) reduces to

$$(\omega, -Ra_T Pr\gamma_0 \Delta b\theta \mathbf{e}_g - 2Ha^2 Prb\Delta b[-\nabla\phi + \mathbf{v}\times\mathbf{e}_B]\times\mathbf{e}_B) + (\mathbf{V}, Ra_T Pr\mathbf{v}) = 0 \tag{35}$$

The adjoint system of equations is summarized in Box III. Using Eqs. (10) and (35), one can finally obtain the following relation:

$$D_{\Delta b}S(b) \equiv (S'(b), \Delta b)_{L_2[0,t_{\max}]} = (\mathbf{v}, \mathbf{V})_{L_2(\Omega_l\times[0,t_{\max}])} = \left(\omega, \Delta b\gamma_0\theta\mathbf{e}_g + 2\frac{Ha^2}{Ra_T}b\Delta b[-\nabla\phi + \mathbf{v}\times\mathbf{e}_B]\times\mathbf{e}_B\right)$$

The gradient of the cost function can therefore be written in terms of the adjoint velocity field as follows:

$$S'(b) \equiv \int_\Omega \left\{\gamma_0\theta(\omega\cdot\mathbf{e}_g) + \frac{2Ha^2}{Ra_T}b\omega\cdot((-\nabla\phi + \mathbf{v}\times\mathbf{e}_B)\times\mathbf{e}_B)\right\} d\Omega \tag{36}$$

This is a compact analytical solution for the gradient of the cost functional in terms of the adjoint velocity in the melt. This result will be used next within a conjugate gradient optimization framework to obtain the desired design solution for $b(t)$ that leads to convection-less solidification growth.

3.4. Numerical implementation

After having obtained an analytical expression for the exact gradient, any of the standard functional minimization techniques can be used for solving the above defined optimization problem in Eq. (9). Here, the non-linear conjugate gradient method (CGM) in L_2 is used to minimize the cost functional $S(b(t))$. This method constructs a sequence $b^0, b^1, \ldots, b^k, \ldots$, to approach the optimum solution $\bar{b}(t)$. The solution of the direct, adjoint and sensitivity problem is realized numerically using the classical SUPG/PSPG method. A deforming finite element formulation to explicitly track the solid–liquid interface is used in the present work. Each mesh (solid/melt) is deformed according to the motion of the freezing interface. Sampath et al. [25] provide details of various computational issues and solution methods that are applied to solve the optimization problem. The entire system of direct, sensitivity and adjoint equations are implemented using an object oriented approach. The interested reader can find details of the implementation and the application of object-oriented techniques applied to adjoint-based inverse design problems in [25,26].

Box III. Adjoint problem to define $\omega(\mathbf{x}, t; b)$, $\psi(\mathbf{x}, t; b)$, $\xi(\mathbf{x}, t; b)$ and $\eta(\mathbf{x}, t; b)$

$$-\frac{\partial\omega}{\partial t} - \mathbf{v}\cdot\nabla\omega + \omega\cdot\nabla\mathbf{v}^T + \nabla\pi - Pr\nabla^2\omega + Ra_T Pr\psi\nabla\theta - Ra_C Pr\xi\nabla c - Ha^2 Prb^2[\mathbf{e}_B(\omega\cdot\mathbf{e}_B) - \omega] - Ha^2 Pr\nabla\cdot(\eta\times\mathbf{e}_B) - Ra_T Pr\mathbf{v} = \mathbf{0}, \quad (\mathbf{x}, t)\in\Omega_l(t)\times[0, t_{\max}]$$

$$\nabla\cdot\omega = 0, \quad (\mathbf{x}, t)\in\Omega_l(t)\times[0, t_{\max}]$$

$$-\frac{\partial\xi}{\partial t} - u\cdot\nabla\xi - Le^{-1}\nabla^2\xi + \omega\cdot\mathbf{e}_g = 0, \quad (\mathbf{x}, t)\in\Omega_l(t)\times[0, t_{\max}]$$

$$-\frac{\partial\psi}{\partial t} - \mathbf{v}\cdot\nabla\psi - \nabla^2\psi + (1-\gamma_0 b)\omega\cdot\mathbf{e}_g = 0, \quad (\mathbf{x}, t)\in\Omega_l(t)\times[0, t_{\max}]$$

$$\nabla^2\eta - b^2\nabla\cdot(\omega\times\mathbf{e}_B) = 0, \quad (\mathbf{x}, t)\in\Omega_l(t)\times[0, t_{\max}]$$

$$\frac{\partial\psi}{\partial n} = 0, \ \frac{\partial\xi}{\partial n} = 0, \quad (\mathbf{x}, t)\in(\Gamma_l(t) - \Gamma_I(t))\times[0, t_{\max}]$$

$$\omega = 0, \ \frac{\partial\eta}{\partial n} = 0, \quad (\mathbf{x}, t)\in\Gamma_l(t)\times[0, t_{\max}]$$

$$\frac{\partial\psi}{\partial n} = 0, \quad (\mathbf{x}, t)\in\Gamma_I\times[0, t_{\max}]$$

$$\frac{\partial\xi}{\partial n} = \xi Le(k-1)\mathbf{v}_\Gamma\cdot\mathbf{n}, \quad (\mathbf{x}, t)\in\Gamma_I\times[0, t_{\max}]$$

$$\omega(\mathbf{x}, t_{\max}) = 0, \ \xi(\mathbf{x}, t_{\max}) = 0, \ \psi(\mathbf{x}, t_{\max}) = 0, \ \eta(\mathbf{x}, t_{\max}) = 0, \quad \mathbf{x}\in\Omega_l(t_{\max})$$

4. Examples

4.1. Pure material/dilute alloy

In this example, the horizontal Bridgeman growth of Antimony doped Germanium is considered. The ampule is 10 cm long and 5 cm wide. The ampule is made of pyrolytic boron nitride (PBN) with a thickness of 1 mm. The furnace closely envelops the crucible. A seed of thickness 5 mm is initially placed on the left side of the configuration and the ampule is filled with charge. The furnace maintains a temperature gradient of 10 K/cm (~25 K/in) in the melt zone and a higher gradient of 30 K/cm (~75 K/in) in the solid zone. The temperature profile increases along the length of the ampule until 40 K superheat is reached after which a constant temperature is maintained. To maintain the stoichiometry of the crystal, arsenic gas at a predetermined pressure is maintained over the free surface of the melt. The thermophysical properties are taken from Adoranto et al. [27] and Oreper et al. [4]. The ampule properties were taken from Barvinschi et al. [28]. A simplified radiation model relating the non-dimensional thermal gradient at

the melt interface and the non-dimensional global temperature is used:

$$\frac{\partial T}{\partial n} = \frac{hL}{K}(T_{\inf}(x) - T) \tag{37}$$

where L is the characteristic length scale of the system and

$$h = \frac{\dfrac{K_{\text{ampule}}}{\delta_{\text{ampule}}}}{1 + \dfrac{K_{\text{ampule}}}{4\delta_{\text{ampule}}\sigma\epsilon T_0^3}}$$

This gives us Neumann boundary conditions for the horizontal bottom wall and the free surface. The crystal is slowly pulled to the left. Directional solidification takes place and a single crystal is produced. To bring out the advantages of using a magnetic gradient on the growth of single crystals a fairly large pulling rate of about 10 cm/h was chosen.

First the horizontal Bridgeman growth of Antimony doped Germanium under standard conditions (normal earth gravity, no magnetic field) was simulated. At early times, the thermal gradients in the originally quiescent melt cause surface tension gradients on the free surface as well as density gradients in the bulk liquid. This leads to combined buoyancy and thermocapillary convection in the fluid. The fluid velocities are maximum at the top free surface in regions close to the moving solid–liquid interface. Continuity of the fluid flow slowly leads to counter-clockwise circulation of the melt filling the entire cavity (Fig. 2). As the solidification process proceeds further, the solid–liquid interface starts to curve, with more solid volume formed at the bottom compared to the top part of the cavity.

The bottom part manages to keep up with the moving imposed thermal gradients at the melt–ampule interface but the aggressive flow towards the interface from the hotter melt causes the front to move very slowly at the top. This trend continues and can be clearly seen in Fig. 3.

The initially flat interface gradually becomes very skewed. In crystal growth a more or less planar interface is desired. This can be achieved either by increasing the thermal gradient or by reducing the pulling rate. Both these measures have major economic consequences. The streamline contours in Fig. 2 clearly show that once the flow pattern has developed (by $t = 0.7$) it remains steady. Notice also that there is a stratification of the isotherms in the middle region of the melt. This would result in the fluctuation of the temperature on the interface and cause the formation of defects and striations.

The isopleths have an almost identical structure to the flow pattern. Initially a high concentration spot is formed at the left top of the melt domain. This is then forced down by the thermocapillary induced convection.

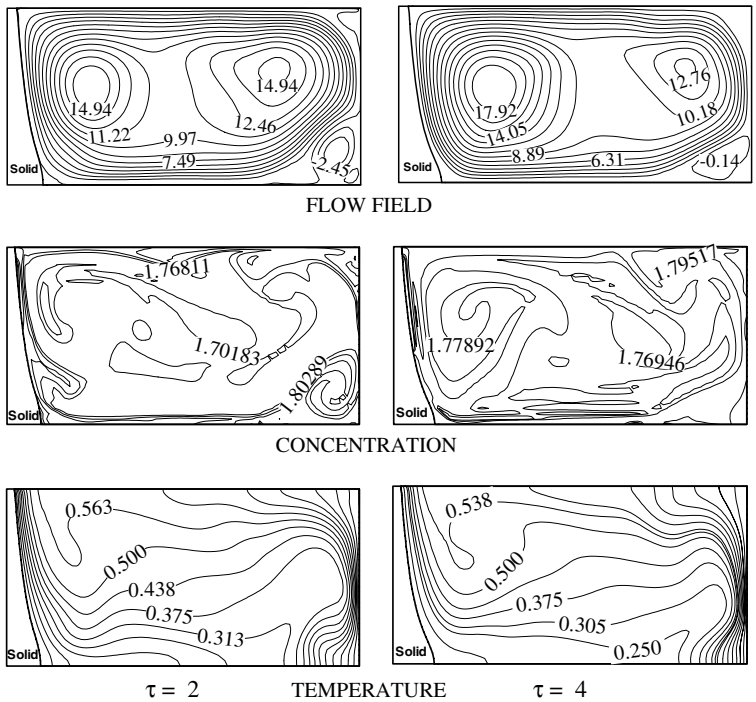

Fig. 2. Calculated contours of streamlines, concentration and temperature at times 2 and 4 for the horizontal Bridgeman growth of SbGe.

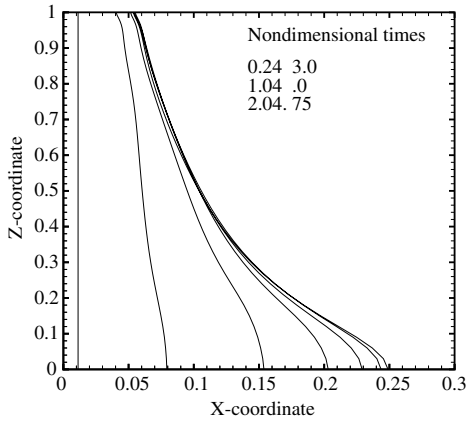

Fig. 3. Solid–liquid interface position with time for the reference SbGe growth with a pulling speed ~10 cm/h.

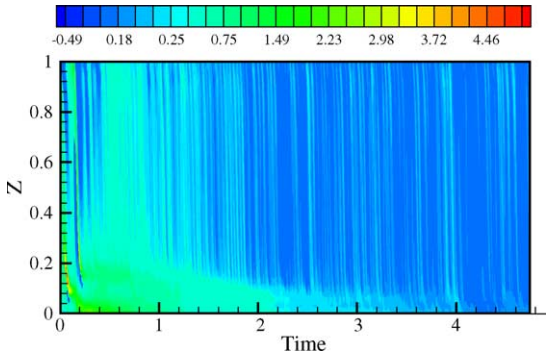

Fig. 4. Calculated history of the solid–liquid interface concentration for the reference problem.

Interestingly, the flow carries the rejected solute down to the bottom of the melt, then across the bottom wall, up the other wall and right back to the interface. In the meantime, the concentration of the solute in the 'flow stream' gradually reduces due to diffusion. This periodic recycling of the dopant at the interface causes a fluctuation in the dopant concentration on the interface and hence on the solid. This phenomenon can be seen in the time history of the concentration at the interface given in Fig. 4. The concentration excess in front of the interface forms until about $t = 1$ after which it is removed by the strong flow patterns. The flow recirculates the solute back to the interface as seen by the fluctuations in the concentration profile with time. Note that these fluctuations become further apart and weaker as time progresses. This is because along with convection the solute is also diffused slowly into the middle relatively quiet zone in the melt.

The crystal growth of GeSb in the horizontal Bridgeman growth configuration at higher crystal pulling rates led to a wavy interface and cyclic fluctuations in the temperature and concentration of the solute at the solid-melt interface. Calculations were carried out for crystal growth under the action of a uniformly imposed magnetic field gradient ($B\frac{\mathrm{d}B}{\mathrm{d}z}$) of about 1.6 T^2/cm. The mean magnetic field resulted in $Ha = 60$. This corresponds to the optimal magnetic field as computed in Section 3.2 superimposed on a given magnetic gradient. Note that these magnetic field conditions correspond to $\gamma = 0.95$. This (sub-optimal) value instead of $\gamma = 1$ was selected here for presentation reasons only in order to allow better visualization of the very weak melt flow results. A weak roll develops at about $t = 0.015$ in the upper left corner of the melt domain. At about the same time, there is a weak flow towards the right at the bottom right of the melt domain. Both these flow patterns develop until about $t = 0.05$. After this, the two patterns begin to interact and the recirculating cell shrinks to form an elongated ellipse near the solidifying interface. This roll fully develops to its maximum strength of 0.6 (compared to the 17.9 in the reference case) by about $t = 0.2$. Thereafter the flow pattern is almost steady. This is clearly seen in the streamline contours given in Fig. 5. The isotherms are nearly parallel to the interface all through the simulation and they closely follow the movement of the externally imposed temperature gradient. This suggests that the heat transfer is nearly conduction-based, with minute local convection effects. The interface growth speed follows the pulling speed. Fig. 6 shows the interface profile with time. Note the significant difference between the interface profiles in the two cases in Figs. 3 and 6. Initially, the melt–crystal interface is planar in both cases. In the reference case, with increasing time, the surface tension induced back flow at the top of the melt causes the interface growth velocity at the top surface to become extremely small. The planar front quickly deteriorates. With the application of the magnetic field superimposed on a magnetic gradient, the interface stays planar with uniform temperature distribution all along the interface. The impact of the application of a magnetic field on the growing front is seen in Fig. 7. The standard deviations of the curvature (deviation from a planar interface) of the preceding two cases (an applied magnetic field gradient and reference case) are plotted as a function of time. Note the significant differences in the standard deviation of the interface for the two cases. Fig. 8 shows the interface concentration profile with time. The concentration is mainly diffusion-based with nearly uniform concentration all throughout the growth run. It must be noted that the concentration on the interface increases very slowly albeit uniformly due to the accumulation of the solute in front of the interface. The slow moving melt could still produce long time-period, low amplitude oscillations in the concentration at the interface (due to recirculation), but this was not observed during the entire growth run.

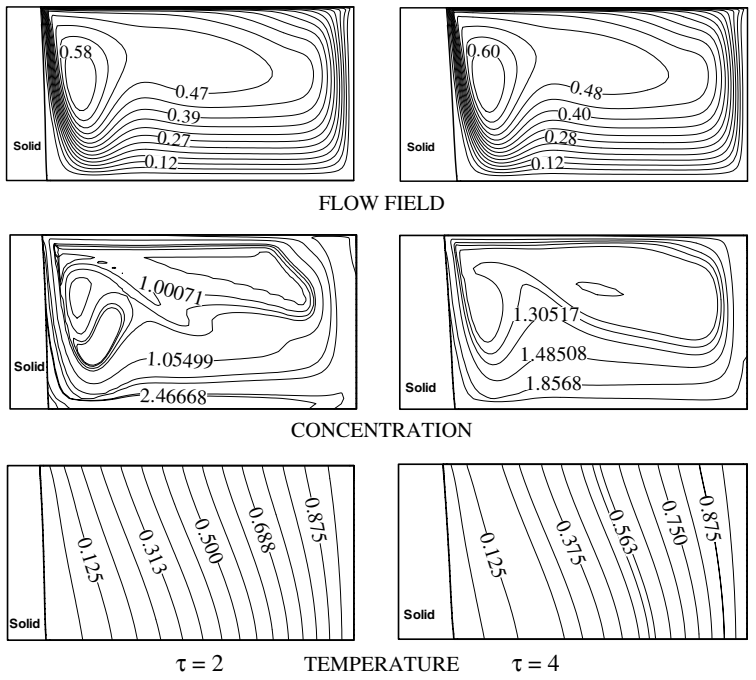

Fig. 5. Calculated contours of streamlines, concentration and temperature at times 2 and 4 for the horizontal Bridgeman growth of SbGe under the action of a magnetic gradient.

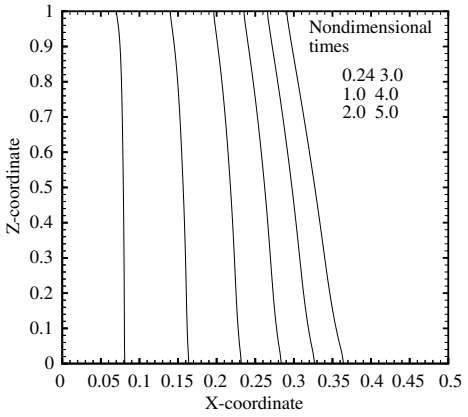

Fig. 6. Solid–liquid interface position with time for SbGe growth with an applied magnetic gradient at a pulling speed ~10 cm/h.

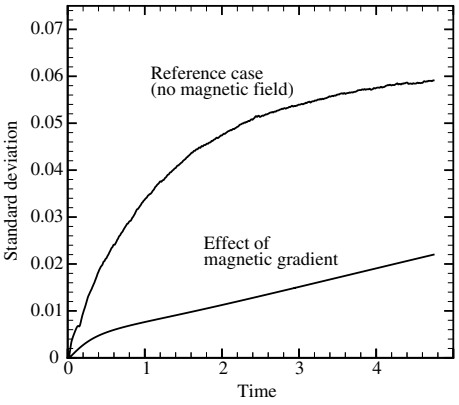

Fig. 7. Deviation of the interface from a planar growth with time.

4.2. Binary alloy

In this example, solidification of a binary alloy in a rectangular cavity of dimensions 2 cm × 2 cm is considered. The physical properties of the system are given as $Pr = 0.007$, $Ra_T = 200000.0$, $Ra_C = 10000.0$, $Le = 1000.0$, $Ste = 0.034$, $R_k = 0.4358$, $R_\alpha = 0.4358$ and $m = -0.001$. The mass magnetic susceptibility of the melt is $\chi = 7.6 \times 10^{-8}$. The initial temperature of the melt was 40 °C above the melting point of the fluid. The left wall is maintained at 40 °C below the freezing temperature for the duration of the simulation. The growth was simulated for a dimensionless time of 0.2. The melt computational domain consisted of 1200 quadrilateral elements and 1271 nodes, while the solid computational domain consisted of 800 quadrilateral elements and 861 nodes. The total simulation consisting of the direct, sensitivity and adjoint problems took around 3.0 h on a Pentium-4 processor based PC.

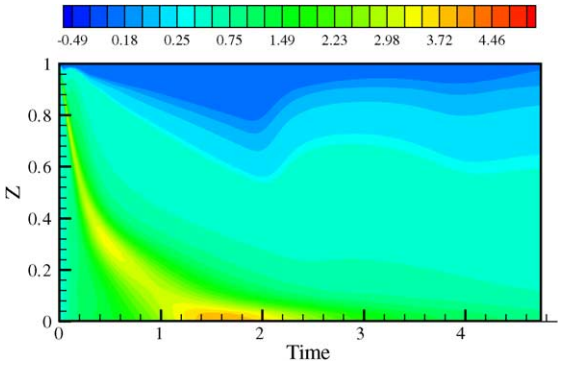

Fig. 8. Calculated history of the solid–liquid interface concentration under the influence of a magnetic gradient.

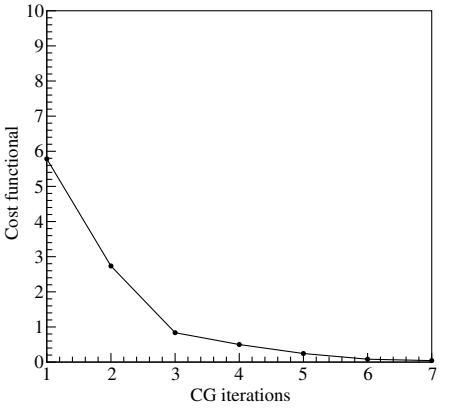

Fig. 9. Cost functional vs. CGM iteration.

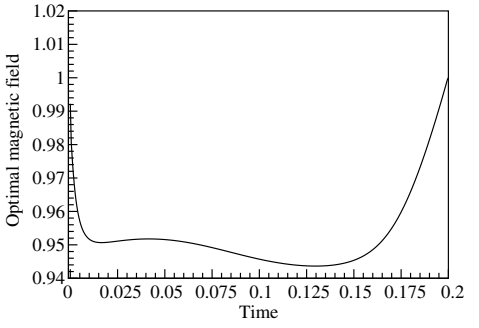

Fig. 10. Plot of optimal magnetic field.

4.2.1. Definition of the inverse design problem

The inverse design problem to be examined here is as follows:

Find the magnetic field $b(t)$ superimposed upon a constant magnetic gradient ($\frac{\partial B}{\partial z} = c$, given) such that convection less growth leading to a vertical interface growth is achieved during the complete growth.

The time domain $[0, t_{\max}]$ is taken with $t_{\max} = 0.2$. This is chosen because beyond this time, the temperature of the melt reaches a temperature close to the freezing temperature and the velocity in the melt region is negligible. Therefore, the end condition difficulty associated with the adjoint method will not be important [20]. An initial guess of $b(t) = \frac{Ra_T - Ra_C}{Ra_T}$ is used to start the CGM iterations. The magnetic field is here non-dimensionalized using a reference field B_{ref} corresponding to $\text{Ha} = 60$. The constant magnetic field gradient is then defined as $B_{\text{ref}} \frac{dB}{dz} = 1.6\ \text{T}^2/\text{cm}$.

Within each CGM iteration, the direct, adjoint and sensitivity problems are solved using the algorithm mentioned earlier. The spatial and temporal discretization remain the same for all three problems. The total number of time steps involved in the solution of each of the direct, sensitivity and adjoint problems is 401. The total computational time for each CGM iteration including the solution of the three subproblems was about 3.0 h. This included considerable time spent on reading/writing data as the adjoint and the sensitivity problems require the direct problem solution at each time step of their solution. The convergence of the CGM is shown in Fig. 9. The computations were stopped after the cost functional reached a specified error tolerance of 5×10^{-4}. The temporal variation of the optimal external magnetic field to be applied is given in Fig. 10.

4.2.2. Validation of the inverse design solution

In order to see how close the desired objectives were met a comparison of the optimal solution with a reference case was made. The reference case involved running the direct problem for no applied magnetic field whereas the optimal solution involved running the direct problem with the magnetic field obtained from the converged CGM optimization scheme (Fig. 10).

To evaluate whether the desired flat interface is obtained the interface positions and shapes for the reference case and the optimal case are shown in Fig. 11. The optimal magnetic field ensures a perfectly planar growth front. To evaluate whether the desired convection-less growth is achieved, isotherms of the reference case as well as the optimal solution are plotted in Fig. 12. Under the action of the optimal magnetic field the isotherms are parallel to the moving front at all times during the growth simulation. The substantial suppression of velocity in the melt is brought out by the streamline contours shown in Fig. 13. The maximum strength of the vorticity reduced from 1.8 to about 0.025. The maximum strength of the velocity reduced from $v_{\max} = 45.82$ to about $v_{\max} = 0.15$. As a consequence of a planar interface and diffusion-dominated growth, the concentration evolution is not affected by convection and is diffusion-based. A comparison of the isochors of

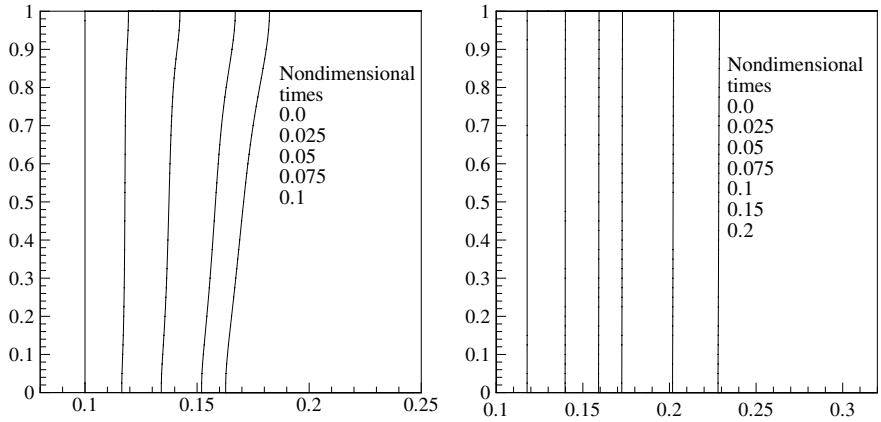

Fig. 11. Interface positions at various times.

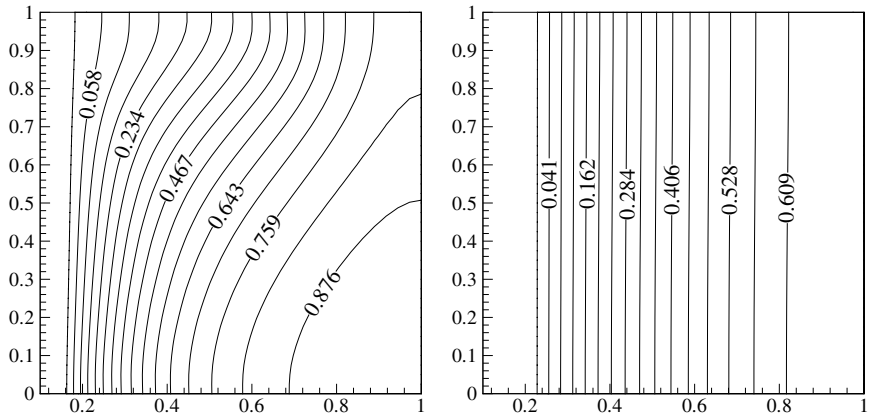

Fig. 12. Comparison of isotherms.

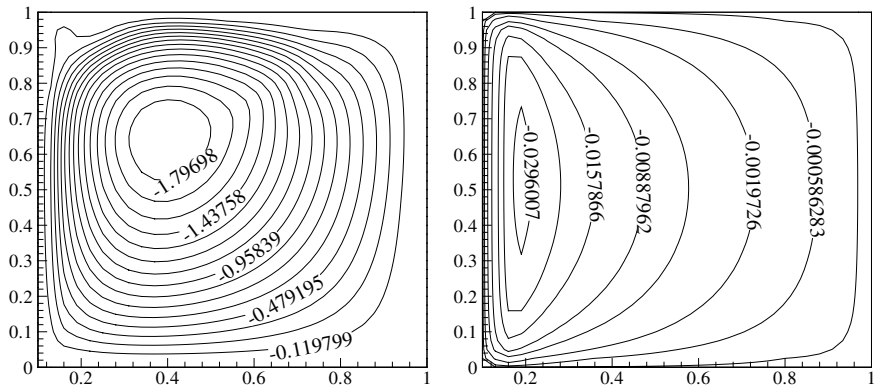

Fig. 13. Comparison of streamline contours.

the two above mentioned cases is provided in Fig. 14. Compare the uniform distribution of the solute along the length of the interface under the action of the magnetic gradient to the isochors for the reference case. The

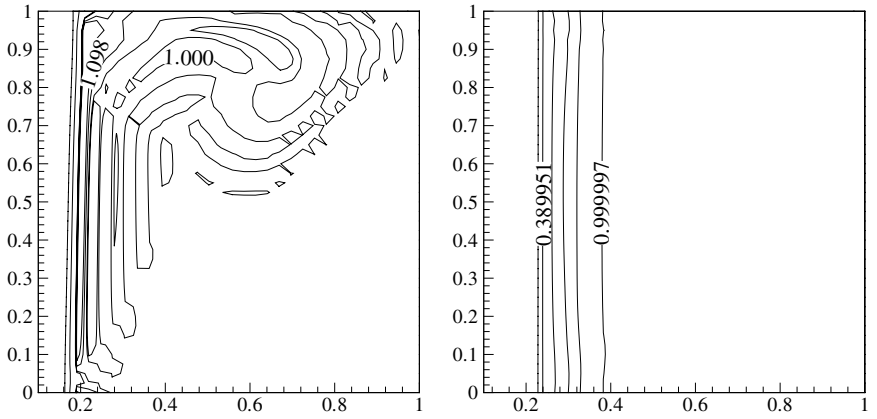

Fig. 14. Comparison of isochors.

solute is uniformly distributed along the length of the interface. This results in a homogeneous distribution of the solute in the solid. The application of the optimal magnetic field along with the superimposed magnetic gradient produces a combination of Lorentz and Kelvin forces which indeed causes a substantial reduction of melt flow thus leading to nearly diffusion-based solidification conditions.

5. Conclusions and suggestions

A systematic continuum formulation using the adjoint method was proposed for the design of solidification processes. The objective was the control of the externally applied magnetic field such that the solidification of the material proceeds in a convection-less environment. An inverse design problem was defined and the exact gradient of the cost functional was obtained using the solution of an adjoint system of equations. The conjugate gradient method in L_2 was used to solve for the optimal magnetic field. The application of the optimal calculated magnetic field along with a superimposed magnetic gradient resulted in a uniform growth of the interface and suppression of temperature and concentration fluctuations in the solid. It has been shown that, through proper application of a magnetic field (and gradient(s)) a state of earth-based reduced gravity growth, resulting in better quality of crystals can be achieved.

The feasibility of the control of solidification through the application of magnetic fields and superimposed magnetic gradients was demonstrated by the examples in Section 4. It is emphasized that the control parameter in this work is only the magnitude of the magnetic field. The present methodology can be further extended to the design of the orientation as well as the magnitude of the magnetic fields. This can be applied to the quality control of various conducting materials in different manufacturing applications like crystal growth and metal casting. Furthermore, real time feedback control of crystal growth and solidification processes is also a very promising issue.

Acknowledgements

The work presented here was funded by the NASA Microgravity Materials Science Program (grant NRA-98-HEDS-05). This research was conducted using the resources of the Cornell Theory Center, which receives funding from Cornell University, New York State, federal agencies, and corporate partners.

References

[1] D.T.J. Hurle, Handbook of Crystal Growth, North-Holland, 1994.
[2] H.P. Utech, M.C. Flemings, Elimination of solute banding in indium antimonide crystals by growth in a magnetic field, J. Appl. Phys. 37 (1966) 2021–2024.
[3] H.A. Chedzey, D.T.J. Hurle, Avoidance of growth-striae in semiconductor and metal crystals grown by zone-melting techniques, Nature 210 (1966) 933–934.
[4] G.M. Oreper, J. Szekely, The effect of a magnetic field on transport phenomena in a Bridgeman–Stockbarger crystal growth, J. Cryst. Growth 67 (1984) 405–419.
[5] S. Motakef, Magnetic field elimination of convective interference with segregation during vertical Bridgeman growth of doped semi-conductors, J. Cryst. Growth 104 (1990) 833–850.
[6] H. Ben Hadid, D. Henry, S. Kaddeche, Numerical study of convection in the horizontal Bridgeman configuration under the action of a constant magnetic field. 1. Two dimensional flow, J. Fluid Mech. 333 (1997) 23–56.
[7] H. Ben Hadid, D. Henry, Numerical study of convection in the horizontal Bridgeman configuration under the action of a constant magnetic field. 2. Three dimensional flow, J. Fluid Mech. 333 (1997) 57–83.

[8] D.H. Kim, P.M. Adornato, R.A. Brown, Effect of vertical magnetic field on convection and segregation in vertical Bridgeman crystal growth, J. Cryst. Growth 89 (1988) 339–356.
[9] M. Gunzberger, E. Ozugurlu, J. Turner, H. Zhang, Controlling transport phenomena in the Czochralski crystal growth process, J. Cryst. Growth 234 (2002) 47–62.
[10] P.J. Prescott, F.P. Incropera, Magnetically damped convection during solidification of a binary metal alloy, Trans. ASME 115 (1993) 302–310.
[11] O. Patzold, I. Grants, U. Wunderwald, K. Jenker, A. Croll, G. Gerbeth, Vertical gradient freeze growth of GaAs with a rotating magnetic field, J. Cryst. Growth 245 (2002) 237–246.
[12] J.K. Roplekar, J.A. Dantzig, A study of solidification with a rotating magnetic field, Int. J. Cast Met. Res. 14 (2001) 79–95.
[13] V. Galindo, G. Gerbeth, W. Von Ammon, E. Tomzig, J. Virbulis, Crystal growth melt flow control by means of magnetic fields, Energy Conv. Manage. 43 (2002) 309–316.
[14] J.W. Evans, C.D. Seybert, F. Leslie, W.K. Jones, Supression/reversal of natural convection by exploiting the temperature/composition dependance of magnetic susceptibility, J. Appl. Phys. 88 (7) (2000) 4347–4351.
[15] J. Huang, D.D. Gray, B.F. Edwards, Thermoconvective instability of paramagnetic fluids in a nonuniform magnetic field, Phys. Rev. E 57 (1998) 5564–5571.
[16] B. Ganapathysubramanian, N. Zabaras, Using magnetic field gradients to control the directional solidification of alloys and the growth of single crystals, J. Cryst. Growth 270 (2004) 255–272.
[17] B. Ganapathysubramanian, N. Zabaras, Control of solidification of non-conducting materials using tailored magnetic fields, J. Cryst. Growth 276 (2005) 299–316.
[18] G. Dulikravich, S.R. Lynn, Unified electro-magneto-fluid dynamics (EMFD)—introductory concepts, Int. J. Non-Linear Mech. 32 (5) (1997) 913–922.
[19] G. Dulikravich, S.R. Lynn, Unified electro-magneto-fluid dynamics (EMFD)—a survey of mathematical models, Int. J. NonLinear Mech. 32 (5) (1997) 923–932.
[20] R. Sampath, N. Zabaras, A functional optimization approach to an inverse magneto-convection problem, Comput. Methods Appl. Mech. Eng. 190 (2001) 2063–2097.
[21] T. Tagawa, A. Ujihara, H. Ozoe, Numerical computation for Rayleigh–Benard convection of water in a magnetic field, Int. J. Heat Mass Transfer 46 (2003) 4097–4104.
[22] T. Tagawa, R. Shigemitsu, H. Ozoe, Magnetizing force modelled and numerically solved for natural convection of air in a cubic enclosure: effect of the direction of the magnetic field, Int. J. Heat Mass Transfer 45 (2002) 267–277.
[23] J.P. Hornak, The Basics of MRI, http://www.cis.rit.edu/htbooks/mri.
[24] S.R. Thomas, L.J. Busse, J.F. Schenck, Gradient coil technology, in: C.L. Partain, R.R. Price, J.A. Patton, M.V. Kulkarni, A.E. James (Eds.), Magnetic Resonance Imaging, Saunders, Philadelphia, 1988.
[25] R. Sampath, N. Zabaras, An object-oriented implementation of adjoint techniques for the design of complex continuum systems, Int. J. Numer. Methods Eng. 48 (2000) 239–266.
[26] R. Sampath, N. Zabaras, An object-oriented implementation of a front tracking FEM for directional solidification processes, Int. J. Numer. Methods Eng. 44 (9) (1999) 1227–1265.
[27] P.M. Adornato, R.A. Brown, Convectiom and segregation in directional solidification of dilute and non-dilute binary alloys: effects of ampule and furnace design, J. Cryst. Growth 80 (1987) 155–190.
[28] F. Barvinschi, I. Nicoara, J.L. Santailler, T. Duffar, Pseudo-transient heat transfer in the vertical Bridgeman crystal growth of semi-transparent materials, Model. Simulat. Mater. Sci. Eng. 6 (1998) 691–700.